Stacking fault energy, yield stress anomaly, and twinnability of Ni_3Al: A first principles study*

Liu Li-Li(刘利利)[a], Wu Xiao-Zhi(吴小志)[a)b)†], Wang Rui(王 锐)[a], Li Wei-Guo(李卫国)[c], and Liu Qing(刘 庆)[b)‡]

[a)] *Institute for Structure and Function, Chongqing University, Chongqing* 401331, *China*
[b)] *College of Materials Science and Engineering, Chongqing University, Chongqing* 400044, *China*
[c)] *College of Aerospace Engineering, Chongqing University, Chongqing* 400044, *China*

(Received 7 January 2015; revised manuscript received 1 February 2015; published online 29 May 2015)

Using first principles calculations combined with the quasiharmonic approach, we study the effects of temperature on the elastic constants, generalized stacking fault energies, and generalized planar fault energies of Ni_3Al. The antiphase boundary energies, complex stacking fault energies, superlattice intrinsic stacking fault energies, and twinning energies decrease slightly with temperature. Temperature dependent anomalous yield stress of Ni_3Al is predicted by the energy-based criterion based on elastic anisotropy and antiphase boundary energies. It is found that p increases with temperature and this can give a more accurate description of the anomalous yield stress in Ni_3Al. Furthermore, the predicted twinnablity of Ni_3Al is also decreasing with temperature.

Keywords: Ni_3Al, stacking fault energy, anomalous yield stress, twinnability

PACS: 71.15.Mb, 71.15.Nc, 71.20.Be, 73.20.At **DOI:** 10.1088/1674-1056/24/7/077102

1. Introduction

The $L1_2$ ordered alloy Ni_3Al is widely used as high temperature structural material because of their superior mechanical properties, such as high strength and resistance to creep.[1–5] The temperature dependent anomalous yield stress, the rise of yield strength with temperature increasing, is observed in Ni_3Al intermetallics.[6,7] This phenomenon has attracted much attention due to the high temperature applications.[8,9] It has been generally accepted that anomalous yield stress is an intrinsic property originated in the structure and properties of superdislocations, and is due to thermally activated cross slip from the (111) primary slip plane to the (010) cross slip plane. The difference in antiphase boundary (APB) energy on (111) and (010) planes is one of the key factors controlling the activation enthalpy of cross slip of a $\langle 110\rangle(111)$ dislocation.[10,11] The anomalies results from the type-I dissociation of $[\bar{1}01]$ superdislocations in (111) and (010) planes according to

$$[\bar{1}01] \rightarrow \frac{1}{2}[\bar{1}01] + \mathrm{APB} + \frac{1}{2}[\bar{1}01], \tag{1}$$

where $[\bar{1}01]$ is the Burgers vector of perfect superdislocations in (111) and (010) planes, which will be dissociated into two $[\bar{1}01]/2$ partial superdislocations in the same planes with an APB between them. Within the Paidar–Pope–Vitek (PPV) model, APB anisotropy ratio $\lambda = \gamma_{\mathrm{APB}}^{\{111\}}/\gamma_{\mathrm{APB}}^{\{010\}} > \sqrt{3}$ is used to predict the cross-slip occurrence in isotropic elastic $L1_2$ alloys.[10] $\gamma_{\mathrm{APB}}^{\{111\}}$ and $\gamma_{\mathrm{APB}}^{\{010\}}$ are the APB energies in (111) plane and (010) plane, respectively. For an anisotropic medium, Yoo pointed out the fact that the effect of elastic anisotropy on the temperature dependence of yield stress is equally important for $L1_2$ alloys.[12] The following energy based criterion should be satisfied

$$p = \left(\frac{3A}{A+2}\right)\frac{\gamma_{\mathrm{APB}}^{\{111\}}}{\gamma_{\mathrm{APB}}^{\{010\}}} > \sqrt{3}, \tag{2}$$

with $A = 2C_{44}/(C_{11} - C_{12})$ the elastic anisotropy ratio. The transition from anomalous to normal temperature dependence of yield strength of $(Ni_{1-x}Fe_x)_3Ge$ has been investigated by Liu *et al.* based on the fact that Ni_3Ge exhibits an anomaly while Fe_3Ge does not.[13] The impacts of 5d transition metals Re and Pt on yield stress anomaly of Ni_3Al are predicted by the APB anisotropy ratio.[14] Tichy *et al.* suggested that the anomaly is also controlled by type-II dissociation of $[\bar{1}01]$ superdislocations in (111) planes according to[15]

$$[\bar{1}01] \rightarrow \frac{1}{3}[\bar{1}\bar{1}2] + \mathrm{SISF} + \frac{1}{3}[\bar{2}11], \tag{3}$$

where $[\bar{1}01]$ perfect superdislocations may also be divided into $[\bar{1}\bar{1}2]/3$ and $[\bar{2}11]/3$ partial superdislocations with superlattice intrinsic stacking faults (SISF) between them, respectively. While type-I dissociation in (111) planes is unstable, type-II dissociation will be favored and it is hard for cross-slip to occur. Superdislocations core structures in $L1_2$ Ni_3Ge, Fe_3Ge,

*Project supported by the National Natural Science Foundation of China (Grant Nos. 11104361 and 11304403) and the Fundamental Research Funds for the Central Universities, China (Grant Nos. CQDXWL2014003 and CDJZR14328801).

†Corresponding author. E-mail: xiaozhiwu@cqu.edu.cn
‡Corresponding author. E-mail: qingliu@cqu.edu.cn

© 2015 Chinese Physical Society and IOP Publishing Ltd

and Ni_3Al are investigated by Mryasov *et al.* within the modified Peierls–Nabarro model with generalized stacking fault (GSF) energy.[16] It is found that type-I dissociation is favored in Ni_3Ge and Ni_3Al, but unstable for Fe_3Ge. In the case of Fe_3Ge, type-II dissociation is energetically preferred. These results are in agreement with the energy condition given by Paidar *et al.*[14,17] Due to the importance of anomalous yield stress, APB energies of Ni_3Al are evaluated from first principles widely at 0 K.[2,3] The APB energies in (010) and (111) planes in nonstoichiometric Ni_3Al have also been measured at different temperatures by TEM.[18–21] Theoretical investigations of the temperature dependence of APB energies are scarce in literature, especially the whole GSF energies which can reflect the dissociation of superdislocations.[7,22–24] Therefore, it is necessary to investigate the temperature dependence of GSF energies of Ni_3Al.

Deformation twinning is another deformation mechanism for plastic deformation in Ni_3Al. The twinning mechanism plays an important role in Ni_3Al with a limited number of independent slip systems, and deformation twinning has been reported by many researchers under various creep loading conditions.[25–27] For example, Viswanathan *et al.*[28] employed the diffraction contrast and high-resolution TEM to investigate the deformation mechanisms during intermediate temperature creep of Ni-based superalloys, and found that microtwinning occurs via sequential movement of identical $1/6\langle 112\rangle$ Shockley partials on successive (111) planes. Xie *et al.*[29] used the molecular dynamics (MD) simulation to explore the dislocation formation and twinning from the crack tip in Ni_3Al. It is well known that the generalized planar fault (GPF) energy curve can predict the preference for twinning in fcc metals and alloys. Recently, there have been many theoretical studies focused on the qualitative dependence of mechanical twinning tendency (twinnability) on the GPF energy curve in fcc metals and alloys.[30–40] The entire GPF energy curve along the pseudo-twinning direction of $1/6\langle 112\rangle(111)$ in $L1_2$ structure alloys has been determined using *ab intio* calculations.[41,42] However, the entire GPF energy curves along the pseudo-twinning direction at different temperatures and, in particular, the temperature dependence of the twinnability, have not yet been reported for Ni_3Al alloy.

In this paper, we employ the first principles methods and quasiharmonic approximation to investigate the GSF energy and GPF energy curves at different temperatures. The main focus is the effects of temperature on elastic constants, anisotropy, APB energies and twinning energies. Based on the above results, temperature dependent yield strength anomaly and twinnability of Ni_3Al are also discussed.

2. Computational method

The Helmholtz free energy of Ni_3Al at a constant volume V and T has three major contributions[43,44]

$$F(V,T) = E_0(V) + F_{\rm el}(V,T) + F_{\rm vib}(V,T), \tag{4}$$

where $E_0(V)$ is the 0 K total energy and $F_{\rm el}$ is the thermal electronic contribution to free energy from finite temperature via integration over the electronic density of state (DOS) following the Fermi–Dirac distribution.[45,46] Both the $E_0(V)$ and $F_{\rm el}$ can be obtained from first principles calculations. $F_{\rm vib}$ is the phonon free energy arising from the lattice vibrations. The phonon free energy within the framework of a quasiharmonic approach can be expressed as

$$F_{\rm vib}(V,T) = \sum_{\boldsymbol{q}\lambda}\left[\frac{1}{2}\hbar\omega_{\boldsymbol{q}\lambda} + k_{\rm B}T\ln(1-{\rm e}^{-\hbar\omega_{\boldsymbol{q}\lambda}/k_{\rm B}T})\right], \tag{5}$$

where $\omega_{\boldsymbol{q}\lambda}$ represents the frequency of the λ-th phonon mode at wave vector $\boldsymbol{q}$, and the sum is over all wave vectors $\boldsymbol{q}$ and over all three phonon branches λ in the first Brillouin zone.

The isothermal elastic constants are defined as the second derivatives of the Helmholtz free energy with respect to strain

$$C^T_{ijkl} = \frac{1}{V}\frac{\partial^2 F}{\partial\eta_{ij}\partial\eta_{kl}}\bigg|_{T,\eta'}, \tag{6}$$

where η' indicates that all other strains are held fixed and $V = V(T)$ is the equilibrium volume at temperature T. There are three independent elastic constants C^T_{11}, C^T_{12}, and C^T_{44} in Ni_3Al. The bulk modulus B_T yield the combinations of the elastic moduli

$$B_T = (C^T_{11} + 2C^T_{12})/3, \tag{7}$$

and determined from the Vinet equation of state[47] corresponding to a pure volume deformation of the lattice. We apply a volume-conserving orthorhombic strain to calculate the difference between C^T_{11} and C^T_{12}

$$\varepsilon(\delta) = \begin{pmatrix} \delta & 0 & 0 \\ 0 & \delta & 0 \\ 0 & 0 & (1+\delta)^{-2}-1 \end{pmatrix}, \tag{8}$$

and the corresponding free energy change is

$$F(V,\delta) = F(V,0) + 3(C^T_{11} - C^T_{12})V\delta^2 + O(\delta^3), \tag{9}$$

with $F(V,0)$ as the free energy of the unstrained structure.

We use a volume-conserving tetragonal strain to determine C^T_{44}

$$\varepsilon(\delta) = \begin{pmatrix} 0 & \delta & 0 \\ \delta & 0 & 0 \\ 0 & 0 & \delta^2/(1-\delta^2) \end{pmatrix}, \tag{10}$$

which leads to the energy change

$$F(V,\delta) = F(V,0) + 2C^T_{44}V\delta^2 + O(\delta^4). \tag{11}$$

In this paper, we use the quasistatic approach proposed by Wang *et al.*[48,49] to calculate the temperature dependence of elastic constants of Ni_3Al. It is based on the assumption

that the temperature dependence of elastic constants is solely caused by thermal expansion. There are abundant experimental evidences[50–52] which support the approximation. The quasistatic approach has the following three steps.[48] The first step is calculating the equilibrium volume $V(T)$ at given T using the first-principles quasiharmonic approximation. In the second step, based on the energy-strain relations Eqs. (8)–(11), we predict that the static elastic constants at 0 K as a function of volume $C_{ij}^T(V(T))$. In the third step, the calculated elastic constants $C_{ij}^T(V(T))$ from the second step are approximated as those at finite temperature. In order to compare with experimental data, the isothermal elastic constants and bulk modulus must be converted to the isentropic elastic constants and bulk modulus by

$$C_{44}^S = C_{44}^T, \tag{12}$$

$$C_{11}^S - C_{11}^T = C_{12}^S - C_{12}^T = B_S - B_T = \frac{TV}{C_v}\alpha^2 {B_T}^2, \tag{13}$$

where C_V is the isochoric heat capacity and α is the thermal expansion coefficient.

The calculations reported in this work are performed with the Vienna *ab initio* Simulations Package (VASP) code.[53] The electron–ion interactions are described by the projector augmented wave (PAW) method[54] and the exchange-correlation functionals are treated by the generalized gradient approximation (GGA) of Perdew–Burke–Ernzerhof (PBE).[55] Convergency of the total energies with respect to the number of $\boldsymbol{k}$-point meshes and the energy cut-off has been checked. Here, the wave functions are sampled on 21×21×21 $\boldsymbol{k}$-point mesh for elastic constants calculations and 21×21×1 for GSF energies and GPF energies calculations based on the Monkhorst–Pack scheme[56] together with the linear tetrahedron method incorporating Blöchl corrections.[57] The energy cut-off of plane wave is set to 500 eV for all calculations. The total energy is converged numerically to less than 10^{-6} eV per atom with respect to electronic self-consistency. We adopt a 48-atom supercell consisting of 10 (111) atomic planes to calculate fault energies to generate GSF energy and GPF energy curves at different temperatures. Between the periodically repeated supercell a vacuum layer with a thickness of 7 (111) atomic planes is added to avoid the fault energy interaction in adjacent cells due to periodic boundary conditions. Due to the ferromagnetic nature of Ni-containing materials, all the calculations are performed within the spin polarization approximation.

Phonon calculations are carried out by the supercell approach as implemented in the PHONOPY package,[58–60] with VASP again the computational engine. The chosen supercell size strongly influences on the thermal properties. Therefore, the adequate supercell size consisting of 3×3×3 unit cells with 108 atoms is chosen to calculate the phonon frequency in Ni_3Al. The forces resulting from displacements of certain atoms in the supercell are calculated by the VASP code with 7×7×7 $\boldsymbol{k}$-point mesh for BZ integrations. The other settings of VASP calculations are the same as those described above. The phonon modes are obtained by using the PHONOPY, which can support the VASP interface to calculate force constants directly in the framework of density-functional perturbation

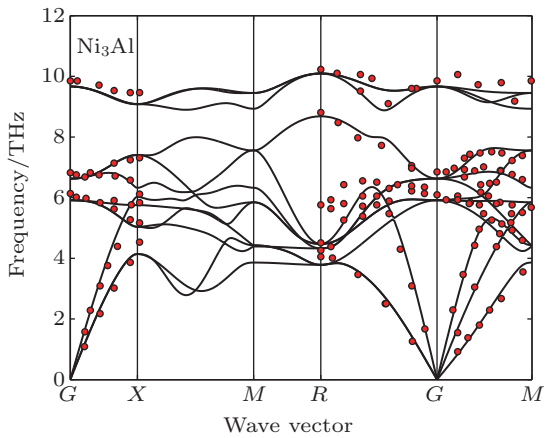


Fig. 1. (color online) Phonon spectrum of the intermetallic compound Ni_3Al. The calculated values are plotted as solid lines and those from the inelastic neutron scattering measurement[64] are plotted as red solid circles.

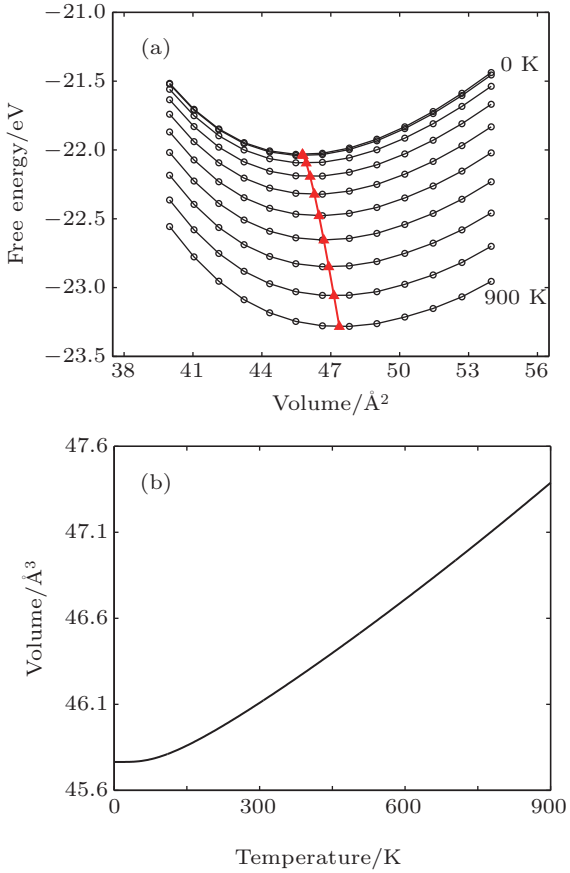


Fig. 2. (color online) (a) The free energy as a function of unit cell volume of Ni_3Al between 0 and 900 K with a step of 100 K and the values depicted by the red triangles are the equilibrium volumes. (b) The equilibrium volumes of Ni_3Al as a function of temperature.

theory (DFPT).[61] Additional details of phonon methodology can be found in Refs. [62] and [63]. Figure 1 represents the calculated phonon dispersion curves for Ni_3Al along several high-symmetry directions in the Brillouin zone together with the room temperature measurements by neutron diffractions of Ni_3Al.[64] A good agreement is observed between calculations and measurements. The method to calculate the temperature dependent lattice constants for Ni_3Al is the same as our calculations for Al, Ni, and Cu.[62,62] Figure 2(a) represents the free energy as a function of unit cell volume of Ni_3Al at every 100 K between 0 and 900 K and the values depicted by the red triangle-up is the equilibrium volume at the corresponding temperature. Obviously, the thermal expansion is obvious as the equilibrium volume is increasing (see Fig. 2(b)).

3. Results and discussion

3.1. Elastic constants and anisotropy

The temperature dependence of elastic constants is important for predicting and understanding the mechanical strength, stability, and phase transitions of a material.[65] In this work, we employ the first-principles quasistatic approach[48,49] to determine the temperature dependent elastic constants of Ni_3Al. The calculated equilibrium lattice constant and elastic constants at $T = 0$ K in comparison with previous theoretical results[66–74] and experimental values[75,76] are tabulated in Table 1. In general, our results are in good agreement with experiments and previous theoretical calculations. Figure 3(a) shows the calculated adiabatic elastic constants in comparison with experimental data from rectangular parallelepiped resonance measurements by Tanaka and Koiwa[77] and Prikhodko.[78] The calculated C_{11}^S, C_{12}^S, and C_{44}^S have been plotted as solid, dash-dot, and dash lines, respectively, and the measured values are plotted as discrete points. The calculated elastic constants are in excellent agreement with experimental data within 5%. The difference may be resulted from neglecting the second-order strain derivative of the Helmholtz free energy. All the calculated values of the elastic constants decrease with temperature increasing and approach linearity at higher temperature and zero slope around zero temperature. The elastic constant C_{11}^S represents elasticity in length. A longitudinal strain causes a change in C_{11}^S. However, the elastic constants C_{12}^S and C_{44}^S are related to the elasticity in shape, which is a shear constant. We find the values of C_{11}^S decrease to the largest extent in the whole temperature range of 0–900 K, and those of C_{12}^S decrease least. The values of C_{11}^S, C_{12}^S, and C_{44}^S decrease by 28.4, 18.8, and 24.2 GPa, respectively. This character indicates that Ni_3Al can keep their mechanical properties in the whole temperature range of 0–900 K and has good high temperature stability. Furthermore, it is noticeable that the requirement of mechanical stability for Ni_3Al in the whole temperature, namely $C_{11} - C_{12} > 0$, $C_{11} > 0$, and $C_{44} > 0$, is satisfied.

Table 1. Calculated equilibrium lattice constant a (Å) and elastic constants C_{ij} (GPa) for Ni_3Al at 0 K compared with previous computed results and experimental data. Note that $C_{ij}^S = C_{ij}^T = C_{ij}$ at 0 K.

Refs.	Method(s)	a	C_{11}	C_{12}	C_{44}
Present	VASP PAW GGA	3.577	228.21	150.85	119.54
[66]	VASP GGA	3.568	229.7	147.5	116.6
[67]	VASP PAW GGA		242.2	151.8	125.4
[68]	LAPW LDA	3.493	226.7	148.1	120.0
[69]	CASTEP GGA	3.574	225.3	157.6	121.1
[70]	CASTEP GGA	3.579	243.8	148.7	123.4
[71]	CASTEP PWPP	3.558	228.4	160.41	123.75
[72]	CASTEP GGA	3.588	230	123	139
[73]	EAM	3.568	216	155	124
[74]	EAM	3.5657	218.3	119.7	102.9
[75]	expt.	3.572	230	150	131
[76]	expt. rectangular parallelepiped resonance method at room temperature	3.56	221.0	146.0	124.0

As is well known, cubic crystals have elastic anisotropy as a result of the fourth rank tensor property of elasticity. The present results for C_{11}^S, C_{12}^S, and C_{44}^S also give the high-temperature elastic anisotropy described by $A = 2C_{44}^S/(C_{11}^S - C_{12}^S)$ of Ni_3Al. Figure 3(b) shows the elastic anisotropy factor, A, plotted as a function of temperature. It is found that the values are between 2.81 and 3.09 in the whole temperature, which are far from unity 1. It indicates that the Ni_3Al alloy in the temperature range of 0–900 K is elastically anisotropic since the anisotropy factor of either smaller or greater than unity represents elastic anisotropy of the crystal. It is known that large values of A can give rise to the driving force acting on screw dislocation to promote cross slip from the (111) plane to the (010) plane. Thus, the relatively high anisotropy factor ($A > 2.5$) in the whole temperature tends to elastically enhance the cross-slip.

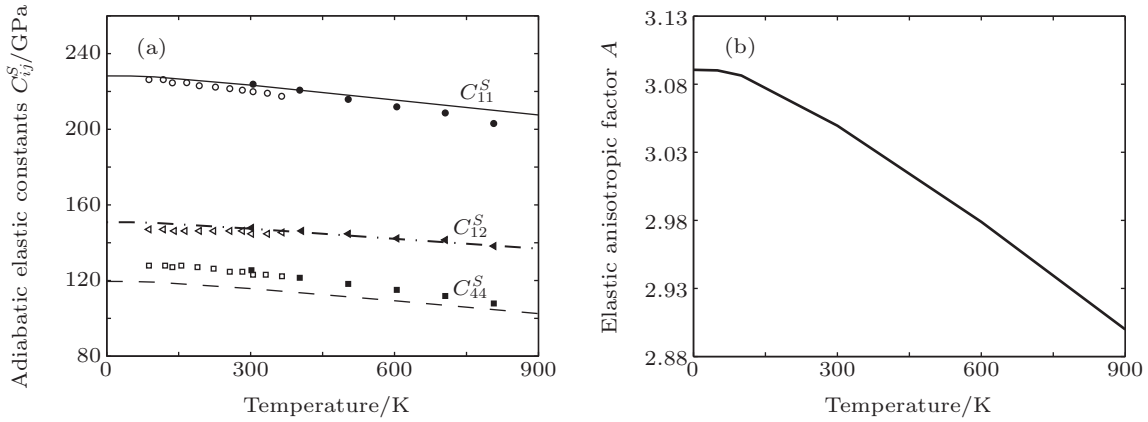


Fig. 3. (a) The calculated adiabatic elastic constants (C_{11}^S: solid line, C_{12}^S: dash-dot line, and C_{44}^S: dash line) of Ni_3Al in comparison with experimental data of Tanaka and Koiwa[77] (C_{11}^S: ○, C_{12}^S: ◁, and C_{44}^S: □) and Prikhodko *et al.*[78] (C_{11}^S: ●, C_{12}^S: ◀, and C_{44}^S: ■). (b) The elastic anisotropic factor A as a function of temperature.

3.2. GSF energy and anomalous yield stress phenomenon

The plastic behavior of Ni_3Al is determined by the dislocation motion and deformation twinning. It is widely accepted that three different types of dislocation dissociations exist in $L1_2$ Ni_3Al. A stable dislocation dissociation is that a $\langle 110\rangle$ superdislocation dissociates into two $1/2\langle 110\rangle$ superpartials bound by APB either on the (111) or (010) plane, type-I dissociation in Eq. (1). Also, the $1/2\langle 110\rangle(111)$ superpartial may further dissociate into two $1/6\langle 112\rangle(111)$ Schockley partials separated by complex stacking fault (CSF) called a metastable dislocation dissociation, namely

$$\frac{1}{6}[\bar{1}\bar{1}2]+\gamma_{\rm CSF}+\frac{1}{6}[\bar{2}11]+\gamma_{\rm APB}+\frac{1}{6}[\bar{1}\bar{1}2]+\gamma_{\rm CSF}+\frac{1}{6}[\bar{2}11].$$

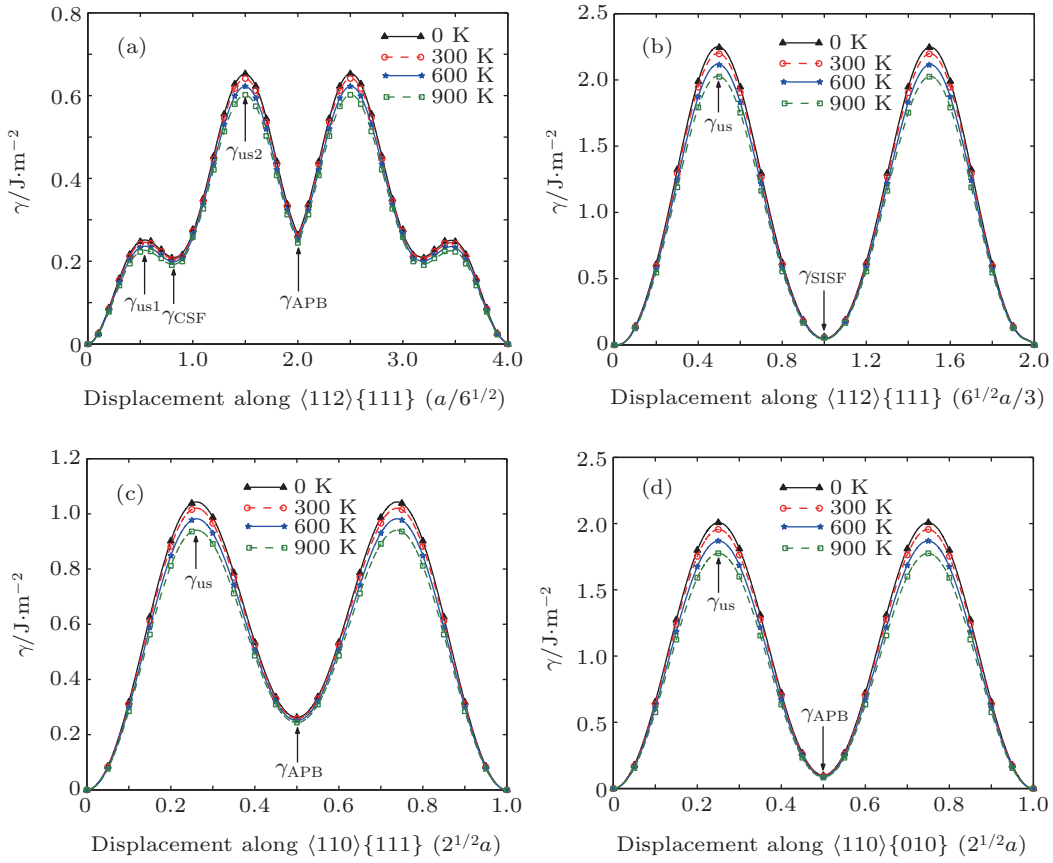


Fig. 4. (color online) The calculated generalized stacking fault energy for Ni_3Al for the temperature range 0–900 K. The discrete points denote the values of first principles calculations and the curves indicate the results from polynomial fitting. (a) Displacement along $\langle 112\rangle\{111\}(a/6^{1/2})$, (b) displacement along $\langle 112\rangle\{111\}(6^{1/2}a/3)$, (c) displacement along $\langle 110\rangle\{111\}(2^{1/2}/a)$, and (d) displacement along $\langle 110\rangle\{010\}(2^{1/2}a)$.

Another stable dislocation dissociation is that the $\langle 110\rangle(111)$ dislocation will also dissociate into two $1/3\langle 112\rangle(111)$ dislocations bound by superlattice intrinsic stacking fault (SISF), type-II dissociation in Eq. (2). In this paper, based on the lattice constant versus temperature relations $a(T)$, all these GSF energy curves in the temperature range of 0–900 K are calculated and plotted in Fig. 4. The change of GSF energies at elevated temperature are mainly caused by volume change due to thermal expansion. The quasiharmonic approach lets one take into account the anharmonicity of the potential at the first order: vibrational properties can be understood in terms of the excitation of the noninteracting phonon. Therefore, the quasiharmonic approximation is usually appropriate if the temperature is lower than the melting point. Therefore, we only calculate the GSF energy curves up to 900 K that is lower than the melting point.

The calculated APB energies, CSF energies, and SISF energies are illustrated in Table 2. Based on these results, we predicted the anomalous yield stress phenomenon by Eq. (2), the energy-based condition. Obviously, all the calculated p at different temperatures satisfy $p > \sqrt{3}$ for Ni_3Al, which indicates that Ni_3Al exhibits the yield strength anomaly. Further, the p changes from 4.888 at 0 K to 5.219 at 900 K. This can give a more accurate description of the anomalous yield stress in Ni_3Al when p increases with temperature.

3.3. GPF energy and twinnability

There are two types of deformation twining in Ni_3Al. One deformation twinning called pseudo-twinning is formed via the sequential motions of identical $1/6\langle 112\rangle$ Shockley partials and the other deformation twinning called anti-twinning is generated by sequential shear of $1/3\langle 112\rangle$ dislocations on successive (111) planes. The GPF energies along the shear direction are evaluated on the two (111) planes. Figure 5 shows the temperature dependent GPF energies curves of Ni_3Al. The first half of each GPF energy curve is evaluated by sliding the upper 6–10 atomic layers relative to atomic layers 1–5 over a distance $a/\sqrt{6}$. The second half is then constructed by displacing the layers numbered 7–10 in the same direction on an adjacent $\{111\}$ plane and a two-layer-thick twinned region is created (see Fig. 6). The first and the second maxima of each curve are the unstable stacking fault (γ_{us1}) and unstable twinning energy (γ_{ut}), respectively. The first and the second minima are stacking fault (γ_{CSF}) and twin stacking fault energy ($2\gamma_{tsf}$), respectively. Numerical values extracted from the curves' extrema are assembled in Table 2. Obviously, all these values decrease with temperature increasing.

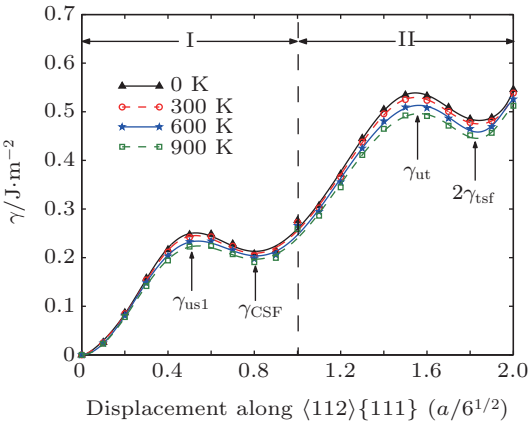


Fig. 5. (color online) The calculated generalized planar fault energy curves for Ni_3Al for the temperature range 0–900 K. The discrete points denote the values of first principles calculations and the curves indicate the results from polynomial fitting.

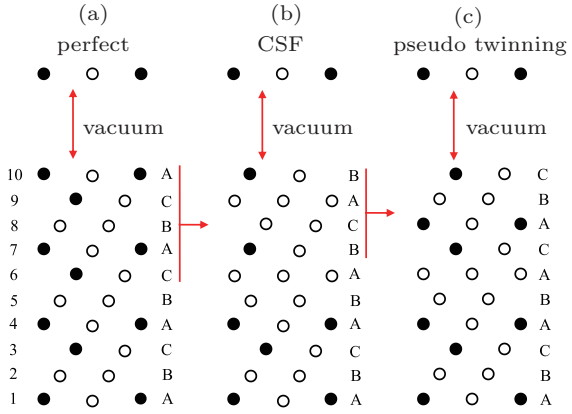


Fig. 6. (color online) A schematic representation of the geometry employed to explain the operations leading to the formation of the complex stacking fault and deformation twinning: (a) perfect structure, (b) complex stacking fault structure imposed by the first displacement operation: layers numbered 6–10 in the upper part, (c) two-layer pseudo twinning structure imposed by the second displacement operation: layers 1–5 in similar fashion. All configurations are separated from the rest by a vacuum.

Previous study has shown that the relative sizes of γ_{us} and γ_{ut} can describe the ease with which an fcc material deforms by twinning relative to deforming by dislocation-mediated slip.[30] According to this analysis, once a leading partial dislocation has been nucleated, whether a subsequent nucleation event will consist of a trailing partial dislocation (i.e., a perfect dislocation) or of a second leading partial on an adjacent slip plane (micro-twin) will be determined by the difference $\gamma_{ut} - \gamma_{us} \equiv \delta_{us}^{ut}$. From Table 2, it shows that the barrier for nucleation of the trailing partial is less than for formation of a microtwin for the temperature range of 0–900 K, $\delta_{us}^{ut} > 0$, inferring that temperature will not switch the dominant deformation mechanism from dislocation-mediated slip to twinning. Further, δ_{us}^{ut} decreases with temperature increasing, this indicates that temperature will make deformation twinning more likely. However, since γ_{ut} is greater than γ_{us} for Ni_3Al at different temperatures, the relative difference criterion can only be used to roughly estimate the twinnability of a material.

Table 2. Stacking fault energies (J/m^2), relative barrier difference δ_{us}^{ut} (J/m^2), twinnability τ of Ni_3Al at different temperatures.

	0 K	300 K	600 K	900 K
$\gamma_{us1}^{\langle 112\rangle\{111\}}$	0.248	0.243	0.234	0.224
$\gamma_{us2}^{\langle 112\rangle\{111\}}$	0.653	0.641	0.622	0.602
$\gamma_{us}^{\langle 110\rangle\{111\}}$	1.038	1.016	0.977	0.936
$\gamma_{CSF}^{\langle 112\rangle\{111\}}$	0.208	0.204	0.197	0.191
$\gamma_{SISF}^{\langle 112\rangle\{111\}}$	0.061	0.059	0.056	0.054
$\gamma_{ut}^{\langle 112\rangle\{111\}}$	0.535	0.525	0.509	0.492
$2\gamma_{tsf}^{\langle 112\rangle\{111\}}$	0.485	0.478	0.465	0.452
$\gamma_{us}^{\langle 110\rangle\{010\}}$	2.008	1.956	1.869	1.776
$\gamma_{APB}^{\{111\}}$	0.263	0.259	0.252	0.244
$\gamma_{APB}^{\{010\}}$	0.098	0.095	0.089	0.083
p	4.888	4.939	5.082	5.219
δ_{us}^{ut}	0.286	0.282	0.276	0.268
τ	0.688	0.686	0.683	0.679

A more thorough treatment of the balance between dislocation-mediated slip and deformation twinning has been proposed by Tadmor and Bernstein[31] in the following form:

$$\tau_a = \left[1.136 - 0.151\frac{\gamma_{sf}}{\gamma_{us}}\right]\sqrt{\frac{\gamma_{us}}{\gamma_{ut}}}, \qquad (14)$$

where γ_{sf} and γ_{us} are replaced by γ_{CSF} and γ_{us1} for the pseudo-twinning in Ni_3Al, respectively. τ_a is a relative measure of the tendency of an fcc metal to undergo deformation twinning: a larger τ_a indicates a greater propensity for twinning. So far, the temperature dependence of the twinnability of Ni_3Al along the pseudo-twinning direction has not been calculated. The computed values of τ_a based on Eq. (14) for Ni_3Al are listed in Table 2. It can be seen that the twinnability parameter of Ni_3Al at 0 K is smaller than those of the fcc pure metals, such as Al ($\tau_a = 0.930$), Cu ($\tau_a = 1.001$), and Ag ($\tau_a = 1.042$).[31] Further, the twinnability of Ni_3Al at different temperatures is much smaller than those of fcc metals.[62] However, the twinnability is similar to that of TiAl ($\tau_a = 0.776$) along its pseudo-twinning direction.[37] From Table 2, it is easy to see that the twinnability of Ni_3Al decreases with the increase of temperature, which has the same change trend with fcc metals.[62,63] However, the twinnability of Ni_3Al with temperature predicted by τ_a and δ_{us}^{ut} are different. It is well-known that deformation twinning becomes more favorable over slip at low temperature and/or high strain rates.[31] In other words, τ_a can more accurately describe the twinnability of a material in comparison with δ_{us}^{ut}.

3.4. Electronic properties

It is generally admitted that the change of charge density intrinsically determines the change of stacking fault energy. Here, the charge density differences on the fifth (010) and (111) planes of faulted and perfect structures are calculated in order to reveal the effect of temperature on the stacking fault energy of Ni_3Al. As shown in Figs. 7(a)–7(d), the significant charge density redistributions can be caused by shifting of the (010) plane at different temperatures. One can easily see that the charge density of 0 K is always larger than that of 900 K for perfect and APB structures. It demonstrates that Ni–Ni and Ni–Al interactions at 0 K are stronger than those at 900 K, all the total energies at 0 K are lower than those at 900 K. A similar charge density redistribution can occur by shifting of the (111) plane at different temperatures. Further, the relative charge density differences between the faulted structure and the perfect structure on the fifth (010) and (111) planes at different temperatures are plotted in Figs. 8(a)–8(d), respectively. One can see that the relative charge density differences at 0 K on the (010) and (111) planes are slightly larger than 900 K, indicating that the fault energies of the (010) and (111) planes at 0 K are slightly higher than 900 K. In other words, the stacking fault energies decrease with temperature increasing.

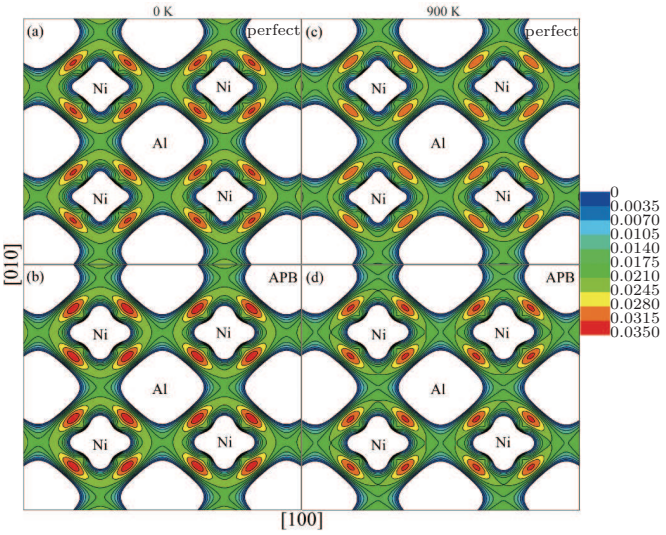


Fig. 7. (color online) The charge distribution difference of perfect and APB structures of (010) plane at different temperatures: (a) 0 K, perfect structure, (b) 0 K, APB structure, (c) 900 K perfect structure, and (d) 900 K, APB structure.

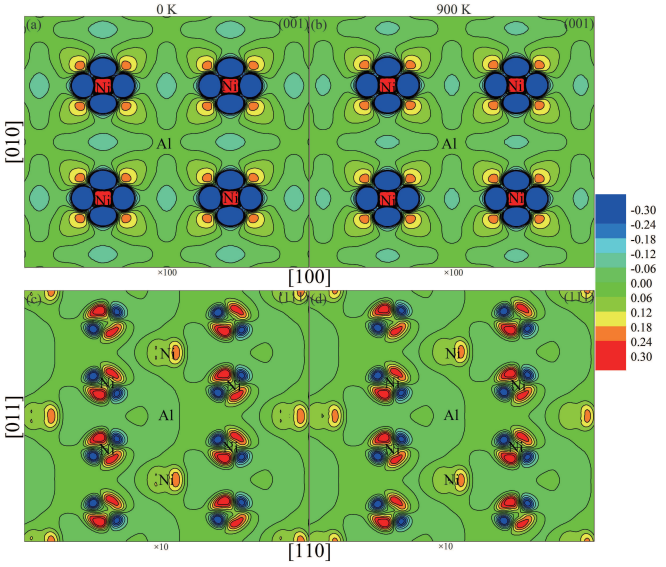


Fig. 8. (color online) Panels (a) and (b) and panels (c) and (d) show the relative charge density differences between the faulted structure and the perfect structure on the fifth (010) and (111) planes at 0 K and 900 K, respectively.

4. Conclusions

In this paper, we employ first principles calculations combined with a quasiharmonic approach to study the effects of temperature on the elastic constants, GSF energies, and GPF energies of Ni_3Al at different temperatures. The APB energies, CSF energies, SISF energies, and twinning energy decrease slightly with temperature. Temperature dependent anomalous yield stress of Ni_3Al is predicted by the energy-based criterion based on elastic anisotropy and APB energies. It is found that p increases from 4.888 to 5.219 ($> \sqrt{3}$) in the range of 0 K to 900 K. This can give a more accurate description of the anomalous yield stress in Ni_3Al. Furthermore, twinnablity of Ni_3Al is also descreasing with temperature.

References

[1] Jiang C, Sordelet D J and Gleeson B 2006 *Acta Mater.* **54** 1147
[2] Chandran M and Sondhi S K 2011 *Model. Simul. Mater. Sci. Eng.* **19** 025008
[3] Yu X X and Wang C Y 2012 *Mater. Sci. Eng. A* **539** 38
[4] Wen Y F, Sun J and Huang J 2012 *Trans. Nonferrous Met. Soc. China* **22** 661
[5] Yang X Y and Hu W Y 2014 *J. Appl. Phys.* **115** 153507
[6] Kumar K, Sankarasubramanian R and Waghmare U V 2015 *Comput. Mater. Sci.* **97** 26
[7] Manga V R, Shang S L, Wang W Y, Wang Y, Liang J, Crespi V H and Liu Z K 2015 *Acta Mater.* **82** 287
[8] Demura M, Golberg D and Hirano T 2007 *Intermetallics* **15** 1322
[9] Yang H, Li Z H and Huang M S 2014 *Modelling Simul. Mater. Sci. Eng.* **22** 085009
[10] Paidar V, Pope D P and Vitek V 1984 *Acta Metall.* **32** 435
[11] Umakoshi Y, Pope D P and Vitek V 1984 *Acta Metall.* **32** 449
[12] Yoo M H 1986 *Scripta Metall.* **20** 915
[13] Liu J B, Johnson D D and Smirnov A V 2005 *Acta Mater.* **53** 3601
[14] Lü B L, Chen G Q, Qu S, Su H and Zhou W L 2013 *Mater. Sci. Eng. A* **565** 317
[15] Tichy G, Vitke V and Pope D P 1986 *Philos. Mag. A* **53** 467
[16] Mryasov O N, Gornostyrev Yu N, van Schilfgaarde M and Freeman A J 2002 *Acta Mater.* **50** 4545
[17] Paidar V, Pope D P and Yamaguchi H 1981 *Scripta Metall.* **15** 1029
[18] Veyssiere P, Yoo M H, Horton J A and Liu C T 1989 *Philos. Mag. Lett.* **59** 61
[19] Morris D G 1992 *Scr. Metall. Mater.* **26** 733
[20] Yu H F, Jones I P and Smallman R E 1994 *Philos. Mag. A* **70** 951
[21] Kruml T, Conforto E, Piccolo B L, Caillard D and Martin J L 2002 *Acta Mater.* **50** 5091
[22] Liu Z G, Wang C Y and Yu T 2014 *Chin. Phys. B* **23** 110208
[23] Li C X, Dang S H, Wang L P, Zhang C L and Han P D 2014 *Chin. Phys. B* **23** 117102
[24] An M R, Song H Y and Su J F 2012 *Chin. Phys. B* **21** 106202
[25] Ardakani A, Mclean M and Shollock B A 1999 *Acta Mater.* **47** 2593
[26] Kakehi K 1999 *Scripta Mater.* **41** 461
[27] Viswanathan G B, Peter M S, Deborah H W and Michael J M 2005 *Mater. Sci. Eng. A* **400–401** 489
[28] Viswanathan G B, Karthikeyan S, Sarosi P M, Unocic R R and Mills M J 2006 *Philos. Mag.* **86** 4823
[29] Xie H X, Wang C Y, Yu T and Du J P 2009 *Chin. Phys. B* **18** 251
[30] van Swygenhoven H, Derlet P M and Froseth A G 2004 *Nat. Mater.* **3** 399
[31] Tadmor E B and Bernstein N 2004 *J. Mech. Phys. Solids* **52** 2507
[32] Siegel D J 2005 *Appl. Phys. Lett.* **87** 121901
[33] Kibey S, Liu J B, Johnson D D and Sehitoglu H 2006 *Appl. Phys. Lett.* **89** 191911
[34] Kibey S, Liu J B, Johnson D D and Sehitoglu H 2009 *Appl. Phys. Lett.* **91** 181916
[35] Muzyk M, Pakiela Z and Kurzydlowski K J 2011 *Scripta Mater.* **64** 916
[36] Li B Q, Sui M L and Mao S X 2011 *J. Mater. Sci. Technol.* **27** 97
[37] Wen Y F and Sun J 2013 *Scripta Mater.* **68** 759
[38] Shang S L, Wang W Y, Zhou B C, Wang Y, Darling K A, Kecskes L J, Mathaudhu S N and Liu Z K 2014 *Acta Mater.* **67** 168
[39] Wang J, Sehitoglu H and Maier H J 2014 *Int. J. Plasticity* **54** 247
[40] Cai T, Zhang Z J, Zhang P, Yang J B and Zhang Z F 2014 *J. Appl. Phys.* **116** 163512
[41] Wu J, Wen L, Tang B Y, Peng L M and Ding W J 2011 *Solid State Sci.* **13** 120
[42] Wang J and Sehitoglu H 2014 *Intermetallics* **52** 20
[43] Moriarty J A, Belak J F, Rudd R E, Sŏerlind P, Streitz F H and Yang L H 2002 *J. Phys.: Condens. Matter* **14** 2825
[44] Wang Y, Liu Z K and Chen L Q 2004 *Acta Mater.* **52** 2665
[45] Sha X W and Cohen R E 2010 *Phys. Rev. B* **81** 095105
[46] Wasserman E, Stixrude L and Cohen R E 1996 *Phys. Rev. B* **53** 8296
[47] Vinet P, Rose J H, Ferrante J and Smith J R 1989 *J. Phys.: Condens. Matter* **1** 1941
[48] Wang Y, Wang J J, Zhang H, Manga V R, Shang S L, Chen L Q and Liu Z K 2010 *J. Phys.: Condens. Matter* **22** 225404
[49] Shang S L, Zhang H, Wang Y and Liu Z K 2010 *J. Phys.: Condens. Matter* **22** 375403
[50] Swenson C A 1968 *J. Phys. Chem. Solids* **29** 1337
[51] Wasserman E F 1990 *Ferromagnetic Materials* (Bushow K H J and Wohlfarth E P eds.) (Amsterdam: Elsevier Science) p. 238
[52] Anderson O L and Isaak D G 1995 *Mineral Physics and Crystallography: A Handbook of Physical Constants* (Ahrens T J ed.) (Washington, DC: The American Geophysical Union) p. 64
[53] Kresse G and Furthmuller J 1996 *Phys. Rev. B* **54** 11169
[54] Kresse G and Joubert D 1999 *Phys. Rev. B* **59** 1758
[55] Perdew J P, Burke K and Ernzerhof M 1996 *Phys. Rev. Lett.* **77** 3865
[56] Monkhorst H J and Pack J D 1976 *Phys. Rev. B* **13** 5188
[57] Blöchl P E, Jepsen O and Andersen O K 1976 *Phys. Rev. B* **13** 5188
[58] Togo A, Chaput L, Tanaka I and Hug G 2010 *Phys. Rev. B* **81** 174301
[59] Togo A, Oba F and Tanaka I 2008 *Phys. Rev. B* **78** 134106
[60] Togo A 2009 *Phonopy*
[61] Kresse G, Marsman M and Furthmüller J VASP the guide
[62] Liu L L, Wang R, Wu X Z, Gan L Y and Wei Q Y 2014 *Comput. Mater. Sci.* **88** 124
[63] Wu X Z, Liu L L, Wang R and Liu Q 2014 *Chin. Phys. B* **23** 066104
[64] Stassis C, Kayser F X, Loong C K and Arch D 1981 *Phys. Rev. B* **24** 3048
[65] Gülsern O and Cohen R E 2002 *Phys. Rev. B* **65** 064103
[66] Wang Y J and Wang C Y 2009 *Appl. Phys. Lett.* **94** 261909
[67] Kim D E, Shang S L and Liu Z K 2010 *Intermetallics* **18** 1163
[68] Osburn J E, Mehl M J and Klein B M 1991 *Phys. Rev. B* **43** 1805
[69] Hou H, Wen Z Q, Zhao Y H, Fu L, Wang N and Han P D 2014 *Intermetallics* **44** 110
[70] Wu Q and Li S S 2012 *Comput. Mater. Sci.* **53** 436
[71] Boucetta S, Chihi T, Chebouli B and Fatmi M 2010 *Mater. Sci. Poland* **28** 347
[72] Sot R and Kurzydlowski K J 2005 *Mater. Sci. Poland* **23** 587
[73] Ravelo R, Aguilar J, Baskes M, Angelo J E, Fultz B and Holian B L 1998 *Phys. Rev. B* **57** 862
[74] Yu S, Wang C Y, Yu T and Cai J 2007 *Physica B* **396** 138
[75] Simmons G and Wang H 1971 *Single Crystal Elastic Constants and Calculated Aggregate Properties: A Handbook* (Cambridge, MA: MIT Press)
[76] Yasuda H, Takasugi T and Koiwa M 1992 *Acta Metall Mater* **40** 381
[77] Tanaka K and Koiwa M 1996 *Intermetallics* **4** S29
[78] Prikhodko S V, Carnes J D, Isaak D G, Yang H and Ardell A J 1999 *Metall. Mater. Trans. A* **30** 2403